BUILD SIMUL (2016) 9: 75–87
DOI 10.1007/s12273-015-0251-6

Validation of numerical simulation tools for wind-driven natural ventilation design

Nuno R. Martins, Guilherme Carrilho da Graça (✉)

Instituto Dom Luiz, Faculdade de Ciências, Universidade de Lisboa, 1749-016 Lisboa, Portugal

Abstract

This paper presents a validation of airflow network (AFN) and computational fluid dynamics (CFD) simulations for a naturally ventilated office building using wind tunnel measurements as the reference for external pressure coefficients and effective airflow rate prediction. The CFD simulation model is also used to study the effect of partially open windows on the effective flow rate. This study also includes a design exercise for a naturally ventilated office building that analyses the differences in predicted average window open area for a typical weather year. The results obtained show that, for simple isolated buildings, CFD can predict pressure coefficients with less than 20% average error. For cases with interfering surrounding buildings or more complex building geometries the average error is less than 40%. Average errors in bulk flow rates are lower: typically less than 25%. The largest errors occur in effective flow rate predictions for cases where the openings are exposed to recirculations and shear driven flows.

Keywords

natural ventilation,
CFD,
simulation validation,
pressure coefficients,
airflow network

Article History

Received: 29 May 2015
Revised: 15 August 2015
Accepted: 20 August 2015

1 Introduction

Natural ventilation (NV) occurs when pressure differences generated by wind or buoyancy forces act on one or more openings in the building envelope. In contrast with the steady energy source used in mechanical ventilation, the variable pressure differences that drive NV systems make sizing of ventilation openings a difficult task (Linden 1999). Throughout history, NV has always remained the preferred choice for residential buildings, while, in commercial buildings, NV went from being the single option to somewhat of a lost art as mechanical ventilation systems became the standard during the second half of the twentieth century. Recently, interest in NV use in commercial buildings has been rising (Carrilho da Graça et al. 2004, 2012). In the milder months of the year, NV is becoming an alternative to mechanical systems due to its potential to reduce ventilation and cooling related energy demand as well as sick building syndrome (Seppänen and Fisk 2002; Dutton et al. 2013).

The hiatus in NV use in commercial buildings resulted in the loss of existing design know-how in a period when comfort and ventilation system performance standards have continuously risen. As a result, currently available simple NV design rules tend to be both overly simplistic and conservative. An example of these limitations can be found in California's Title 24 (California Building Standards Commission 2013) recommendation of a 5% minimum ratio between floor and facade opening area and the 20 ft maximum natural flow penetration rule. This rule limits the use of natural ventilation to office areas that are less than 20 ft (6 m) away from a facade with operable windows. Yet, it is possible that, in tall rooms, single sided natural displacement ventilation may provide adequate fresh air beyond 6 m with a window opening area that is less than 5% (Carrilho da Graça et al. 2015). To overcome these restrictions and test new design possibilities engineers need improved airflow simulation tools or, when available, reliable measurements. These tools must incorporate a wide range of factors that affect the variations in pressure distribution around and inside the building, such as building and surrounding geometry, incoming wind and differences between internal and external temperature (Montazeri and Blocken 2013).

E-mail: gcg@fc.ul.pt

Abbreviations

AFN	airflow network
CFD	computational fluid dynamics
CV	cross ventilation
LES	large eddy simulation
NV	natural ventilation
RANS	Reynolds-averaged Navier–Stokes equations
WT	wind tunnel

List of symbols

A	window area (m^2)
CFL	Courant–Friedrichs–Lewy number
C_D	discharge coefficient
C_p	wind pressure coefficient
c_p	air specific heat (J/(kg·K))
K	pollutant concentration
K_0	initial pollutant concentration
N	number of measured values
n	number of building apertures
p	pressure (Pa)
R^2	coefficient of determination
T	temperature (°C)
T_0	initial temperature (°C)
T_{base}	outdoor base temperature (°C)
t	time (s)
U_{max}	maximum fluid velocity (in CFD) (m/s)
u_{wind}	wind velocity (m/s)
V	room volume (m^3)
$\dot{V}$	airflow rate (m^3/s)
x_{min}	minimum spatial grid step (m)
y_i	measured value
$\hat{y}_i$	predicted value
$\overline{y}_i$	average measured value
Δ	variation
ρ	air density (kg/m^3)

Measurements can be performed in scaled wind tunnel models or, in rare instances, in full-scale. Both methods have known limitations. When possible, full-scale measurements would be the ideal choice; however controlling boundary conditions is very difficult (Zhou et al. 2014; Lo et al. 2013; Belleri et al. 2014). In contrast, scaled building model boundary layer wind tunnel (WT) experiments can have clearly defined boundary conditions. Still, this approach can be time-consuming and expensive (Labat et al. 2013). Further, downscaling the building apertures is difficult: scaled model walls tend to be disproportionally thick and apertures are usually modeled as fully open holes with variable area. These crude approximations affect the aperture pressure loss (Heiselberg et al. 2001) and fail to capture the inflow deflection produced by partially open windows (Heiselberg et al. 2002). In spite of these limitations, scaled WT measurement is the reference method for building natural ventilation modeling (Cochran and Derickson 2011), particularly for determining pressure coefficients and effective flow rates in buildings with fully open windows.

Numerical simulation approaches for NV design range from simple airflow network models (AFN) to complex three-dimensional computational fluid dynamics simulations (CFD, see Table 1). AFN models are based on the orifice flow equation and have low computation time and high numerical stability (Axley 2007). As a result, these models are commonly used to predict bulk NV airflow in hourly thermal simulation software tools (Carrilho da Graça et al. 2012; Crawley et al. 2001). In AFN models, wind pressure effects in each external opening are modeled using pressure coefficients (C_p) that can be obtained from WT measurements or CFD simulations. In contrast with AFN, CFD is able to produce whole flow field data in full-scale. For this reason, CFD simulations tend to have high computation time and variable numerical stability. Further, CFD simulation results are sensitive to a large number of user-defined computational parameters. Although there have been continuous improvements in CFD tools the typical accuracy of this methodology when applied to NV remains an open issue (Bitsuamlak 2006; Blocken 2014; Chen 2009; Jiang et al. 2003). In spite of this, CFD has reached a development stage that makes it a candidate for use as an accessible and flexible virtual wind tunnel, either producing the pressure coefficients that are required for AFN models or the whole flow field for particular wind directions and window configurations.

This paper presents a validation of AFN and CFD simulations for a naturally ventilated office building using WT measurements as the reference for external pressure coefficients and effective airflow rate prediction. This validation focuses specifically on wind driven cross ventilation with no buoyancy effects. Further, the shear driven flows that occur in a limited set of incoming wind directions are not analyzed in detail in this study. In addition to the validation, this study compares the average window open area required to meet a given target flow rate that is predicted by the two numerical models for a typical weather year. Finally, the CFD simulation model is used to study the effect of partially open windows on the effective flow rate (an effect that typical WT studies fail to capture). The next section of this paper presents a review of existing comparisons between

Table 1 Natural ventilation modeling methods analyzed in this paper

Method	Predicted variable	Requirement	Effort/time
Wind tunnel (WT)	External pressures Effective airflow rates	Wind tunnel Scaled model	High
Computational fluid dynamics (CFD)	Whole field data (pressures, velocities, etc.)	CFD model	Medium
Airflow network (AFN)	Bulk airflow rates	Pressure coefficients (C_p from WT or CFD)	Low (when C_p is available)

CFD, AFN and WT studies. This section is followed by a description of the methodology and case study used in this study. The following section presents the pressure coefficients and effective airflow rate predictions. The last section of this paper assesses the impact of window geometry on effective flow rates.

2 Bibliographic review

This bibliographic review is divided in four sections. The first two sections present an overview of the two building ventilation numerical simulation methods that will be analyzed in this paper. The third and fourth sections present existing comparisons between CFD, AFN, and WT, for three relevant flow parameters:

- Pressure coefficients: comparison between CFD and WT.
- Effective airflow rates: comparison between CFD and WT.
- Bulk airflow rates: comparison between CFD and AFN.

The accuracy of the numerical simulation methods will be assessed using the coefficient of determination, R^2, (Eq. (1)) and an average normalized error (Eq. (2)), defined as follows:

$$R^2 = 1 - \frac{\sum_{i=1}^{N}(y_i - \hat{y}_i)^2}{\sum_{i=1}^{N}(y_i - \bar{y})^2} \quad (1)$$

$$\text{Average error} = \frac{\sum_{i=1}^{N}\frac{|y_i - \hat{y}_i|}{N}}{\sum_{i=1}^{N}\frac{|y_i|}{N}} \quad (2)$$

2.1 Computational fluid dynamics (CFD)

The standard CFD approach for building natural ventilation design is RANS (Reynolds-averaged Navier–Stokes) combined with different variants of the k–ε turbulence model (Chen 2009). This approach is the preferred choice due to its robustness (Cheung and Liu 2011) and tested precision for different building ventilation applications (Chen 1995). In addition to the standard k–ε model, variants such as the RNG k–ε model (Glória Gomes et al. 2005), the realizable k–ε model (Teppner et al. 2014), and the k–ω model (Nikolopoulos et al. 2012) are also being increasingly used in NV applications. These models address several known limitations in the standard k–ε model, namely, overestimation of turbulence energy (Tominaga et al. 2008a) and difficulty in describing flows close to surfaces (Evola and Popov 2006). In the future, RANS may be replaced by large eddy simulation (LES), a more detailed approach, based on space filtering of turbulent structures and explicit dynamic modeling of the large eddies. For the time being, RANS is preferred over LES due to its significantly lower computational cost (Jiang and Chen 2002; Nikas et al. 2010).

2.2 Airflow network (AFN) models

AFN models use a network of interconnected nodes connected by nonlinear pressure dependent flow resistances (Asfour and Gadi 2007; Axley 2007). A typical AFN model will have one node for each building zone plus a variable number of outside nodes. The bulk airflow rate for a given aperture is calculated from the pressure difference between the zones that the aperture connects. For wind-driven airflow the incoming flow rate can be calculated using the following variant of the aperture Eq. (3) (Shen et al. 2012):

$$\dot{V} = A \times C_D \times u_{wind} \times \sqrt{\Delta C_p} \quad (3)$$

A discharge coefficient (C_D) of 0.6 was used (Shen et al. 2012). The non-linear system of n equations that results from applying mass conservation to the building zones and n building apertures is then solved numerically. An average pressure coefficient was calculated for each side of the building and used within a single equation. These pressure coefficients (C_p), are defined as the ratio of local wind-driven static pressure and the incoming wind pressure, as shown in Eqs. (4) and (5) (Awbi 2003):

$$C_p = \frac{p_{local}}{p_{wind}} \quad (4)$$

$$p_{wind} = \frac{\rho \times u_{wind}^2}{2} \quad (5)$$

2.3 CFD accuracy assessment

2.3.1 *Pressure coefficients*

This review identified eight previous studies that compare pressure coefficients obtained from CFD with WT measurements (Table 2). The average errors found in these studies vary between 7% and 47% and the R^2 values between 0.420 and 0.995. A more detailed analysis reveals a higher agreement for cases with normal or near normal incoming wind (the first six studies in Table 2 (Calautit and Hughes 2014; Kobayashi et al. 2010; Seifert et al. 2006; Montazeri and Blocken 2013; van Hooff et al. 2011; Liu et al. 2013). Cases with more complex building geometry or a wider range of incoming wind angles display a lower accuracy (Glória Gomes et al. 2005), with the largest error found in a case with several near buildings and multiple incoming wind angles (Zhang and Gu 2008).

2.3.2 *Effective airflow rates*

Due to non-homogeneous mixing between the airflow entering the room and existing room air, effective flow rates are lower than the bulk airflow through the building's openings. In NV design, CFD simulations are often used to calculate the effective airflow rate in specific room locations. The most commonly used methodology to calculate the effective flow rate is the concentration decay method. Starting with an evenly distributed non-buoyant pollutant concentration this method determines the effective flow rate by finding the best fit between pollutant decay curve and the solution of the concentration decay (Eq. (6)) (Awbi 2003):

$$K(t) = K_0 \times \exp\left(-\frac{\dot{V}}{V} \times t\right) \tag{6}$$

The results of two existing studies that compare CFD and WT effective airflow rate are shown in Table 3. Due to the higher complexity that results from the inclusion of internal partitions the second case has much lower correlation. Further, detailed analysis of the results, not shown here, revealed that, as in the case of pressure coefficients, smaller incoming wind angles (0°–30°) lead to lower discrepancies: as the incoming wind angle approaches 90°, the airflow deviates from cross-ventilation, and begins to resemble

Table 2 R^2 and average error between WT and CFD pressure coefficients for previous studies

Reference	Case study/turbulence model	Wind angle (normal = 0°)	R^2	Average error (%)
Calautit and Hughes 2014	Isolated wind tower Standard k–ε model	0°	0.995	7
Kobayashi et al. 2010	Isolated real-shaped building Reynolds stress model	0°	0.995	9
Seifert et al. 2006	Cube-shaped isolated building RNG k–ε model/standard k–ε model	0°	0.972 (RNG) 0.847 (standard)	13 (RNG) 33 (standard)
Montazeri and Blocken 2013	Isolated real-shaped building Realizable k–ε model	0° and 45° to surface	0.985	14
van Hooff et al. 2011	Venturi-shaped roof RNG k–ε model	0° to 45° to surface, 15° interval	0.974	11
Liu et al. 2013	Isolated real-shaped building RNG k–ε model/standard k–ε model	0° and 45° to surface	0.960 (RNG) 0.912 (standard)	21 (RNG) 25 (standard)
		Average error (incoming wind angles between 0° and 45° to surface)		**17**
Glória Gomes et al. 2005	L and U-shaped isolated buildings RNG k–ε model	0°, 45° and 180° to surface (three)	0.932	23
Zhang and Gu 2008	Building with near interference RNG k–ε model	0° to 345° to surface, 22.5° interval (sixteen)	0.420	47
		Average error (studies including all incoming wind angles)		**35**

Table 3 R^2 and average error between wind tunnel and CFD effective flow rates for previous studies

Reference	Case study/turbulence model	Wind angle (normal = 0°)	R^2	Average error (%)
Shen et al. 2012	Isolated building Standard k–ε model/RNG k–ε model	0° to 90° to surface, 10° interval (ten)	0.613 (standard) 0.541 (RNG)	32 (standard) 33 (RNG)
Nikolopoulos et al. 2012	Cube-shaped isolated building with inner divisions Standard k–ω model	0° to 90° to surface, 30° interval (four)	–0.296	29
			Average error	**31**

shear-driven ventilation. Due to the difficulty of CFD to model this type of ventilation, the disparity between CFD and WT effective flow rates increases for this cases.

2.4 CFD and AFN accuracy assessment: Bulk airflow rates

Bulk flow rates are usually not measured in WT studies because it is impossible to insert a velocity sensor in the small openings used, without affecting the flow. Further, a set of measurements in known locations in the window plane would be required for an accurate flow measurement.

This review identified two studies comparing flow rates predicted by CFD with AFN predictions (using WT pressure coefficients), which are presented in Table 4. As in the previous cases, configurations with incoming wind angles that are closer to normal incidence (Asfour and Gadi 2007) have significantly better results: 6% average error, versus 28%–34%.

3 Case study and methodology

This section presents the case study used in this paper, a two-story 940 square meters office building located in Alameda, California (15 km from San Francisco). The focus of this validation study is the open plan, 109 square meters office room on the second floor of the building shown on the right hand side of Fig. 1. The following sections describe the models used to simulate this room and the methodology employed in this study.

3.1 Wind tunnel measurements

The wind tunnel model used in this study was built and measured by CPP Wind (2015). The model is a 1:70-scale replica of the building and its immediate surroundings, within a one hundred meters ratio. The modeled room has four openings, labeled W1 to W4, as can be seen in Fig. 2.

Table 4 R^2 and average error between AFN and CFD bulk flow rates for previous studies

Reference	Case study/turbulence model	Wind angle (normal = 0°)	R^2	Average error (%)
Asfour and Gadi 2007	Cuboid-shaped isolated buildings WT C_p Standard k–ε model	0° and 45° to surface (two)	0.944	6
Shen et al. 2012	Isolated building WT C_p Standard k–ε model/RNG k–ε model	0° to 90° to surface, 10° interval (ten)	0.679 (standard) 0.688 (RNG)	28 (standard) 34 (RNG)
			Average error	**23**

Fig. 1 Aerial view (left), wind tunnel model of the main building and surrounding buildings (right)

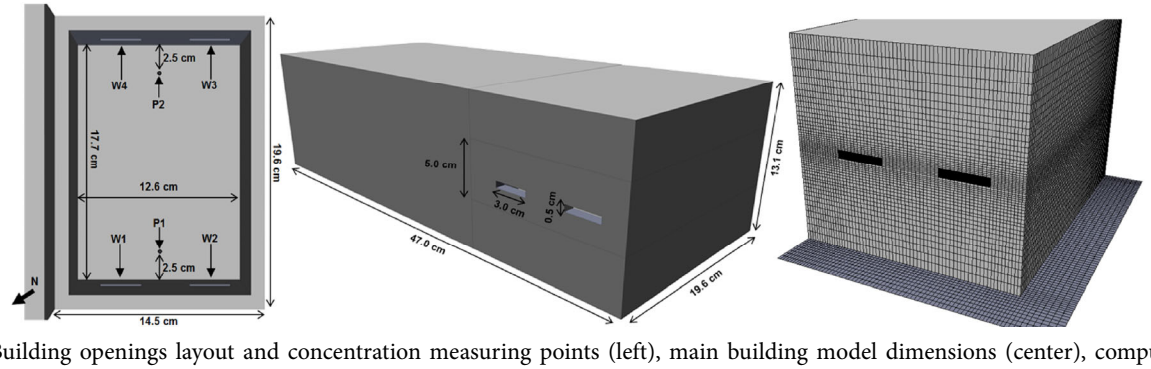

Fig. 2 Building openings layout and concentration measuring points (left), main building model dimensions (center), computational grid surrounding the main building openings (right)

Each window has an opening area of 1.66 cm^2, leading to wall porosity of 0.54%. To simulate the variable incoming wind direction (0° to 345°, in 15° intervals) the model is placed on a rotary table. A logarithmic incoming wind profile was used (Richards and Norris 2011), with a wind velocity of 8.148 m/s at 0.202 m and a surface roughness of 4.36 mm (Table 5). Similarity requirements were ensured to be in accordance with the EPA fluid modeling guidelines (United States Environmental Protection Agency 1981) and with Cermak (1971, 1975, 1976).

Table 5 Wind tunnel inflow velocity and turbulence intensity profiles

Height (m)	Velocity (m/s)	Turbulence intensity (%)
0.076	6.464	23.4
0.103	6.892	22.2
0.126	7.469	22.5
0.154	7.770	21.9
0.202	8.148	19.1
0.253	8.570	18.8
0.305	8.892	18.2
0.405	9.520	18.0
0.510	10.009	16.3
0.610	10.337	16.4
0.814	11.347	15.9
1.066	12.046	13.5
1.218	12.442	12.2

Wind pressure coefficients were measured using an array of six flush surface pressure taps along the edge of each opening. Effective airflow rates were calculated for each wind direction using the concentration decay methodology. Pollution concentration was monitored at 200 Hz with two fast flame ionization detectors (FFID), located at two points, P1 and P2, positioned at mid-height, mid-width and 2.5 cm away from walls.

As can be seen in Fig. 4, pollutant concentration between both measurement points differs during the filling phase (when the non-buoyant pollutant source is active). Once the source is removed, the pollutant concentration within the building model becomes more homogeneous, resulting in a difference of less than 10% between both points for most incoming wind directions.

3.2 CFD simulations

The CFD model (Figs. 2 and 3) used in this study is a virtual full-scale replica of the wind tunnel model (Fig. 1). The simulations were performed using the commercial CFD package PHOENICS 3.6 (CHAM Ltd. 2012). The simulation models were set up in accordance with the recommendations of Tominaga et al. (2008b) and Franke et al. (2007), and are described in more detail below.

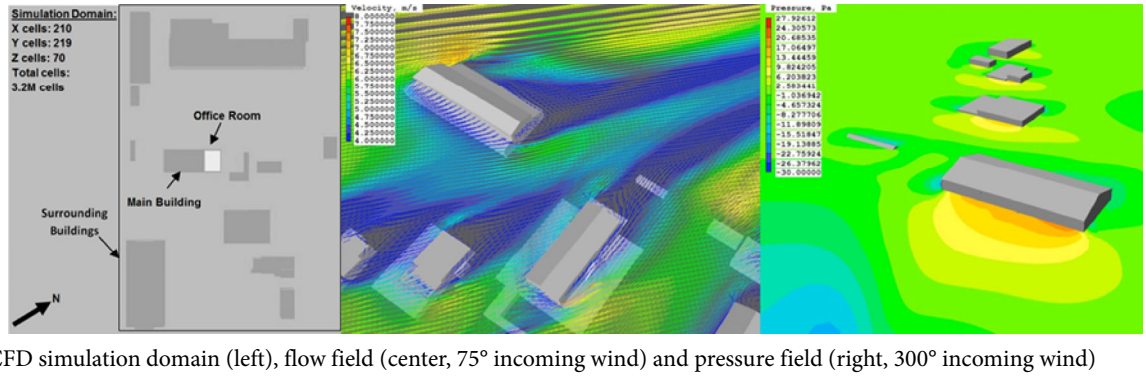

Fig. 3 CFD simulation domain (left), flow field (center, 75° incoming wind) and pressure field (right, 300° incoming wind)

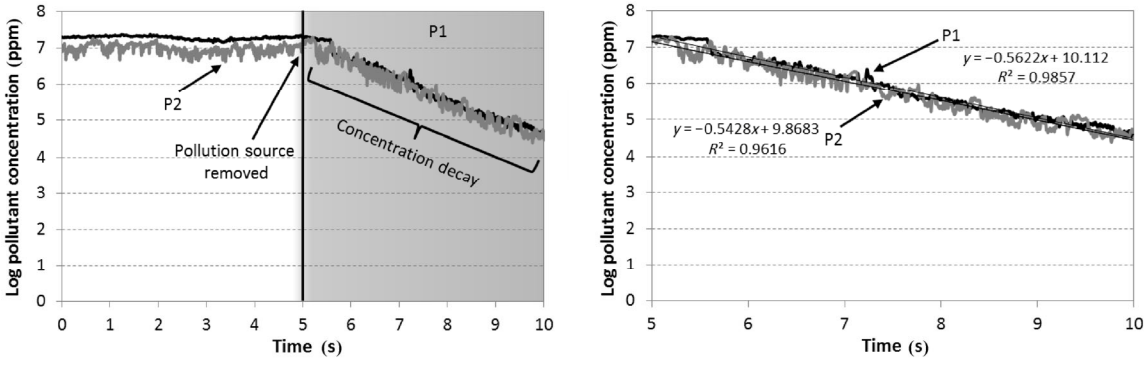

Fig. 4 Pollution concentration within the WT building model over time (left, 15° incoming wind) and focus on concentration decay (right)

3.2.1 Computational domain

The recommended minimum 15 H distance (H being the height of the building) between the model and the outlets is kept around the built area, easily allowing the rotation of the incoming wind. The use of a 15 H distance, combined with a domain height of 6 H (higher than the recommended minimum of 5 H) led to a blockage ratio of less than 0.5%, lower than the recommended maximum of 3%.

3.2.2 Grid and time resolution

The simulation's spatial grid must be sufficiently detailed to accurately describe the airflow. However, an excessively detailed grid requires a longer simulation time, without providing any increase in accuracy. Thus, further exploratory runs were performed to achieve an optimal spatial discretization. Three simulation grids, with 2.8, 3.2 and 3.9 million cells (named low, medium and high resolution, respectively) were tested to calculate the bulk airflow rate for four incoming wind directions. The results of these test runs are presented in Table 6.

As can be seen, a lower spatial resolution carries differences (up to 3%) regarding the airflow rate, while the higher resolution brings no significant changes (less than 1%) and requires a lengthier simulation time. Thus, the medium resolution grid was chosen for the subsequently described simulations.

In addition to an adequate spatial grid, transient simulations require a time step that avoids excessive simulation time while still providing realistic results. A conservative approach to define this time step is given by Eq. (7):

$$\Delta t = \mathrm{CFL} \times \frac{\Delta x_{\min}}{U_{\max}} \tag{7}$$

The Courant–Friedrichs–Lewy parameter (CFL) should have a maximum value of one, as indicated by Anderson Jr. (1995). This limit ensures that the simulation fluid can only move a maximum of one grid step per time step. Failure to meet this requirement might lead to an inaccurate fluid movement, as intermediate fluid positions are not simulated. Regarding the present simulations, the value of this parameter was set to one.

Table 6 Bulk airflow rates regarding grid resolution exploratory runs

Wind direction (°)	Low resolution (dm³/s)	Medium resolution (dm³/s)	High resolution (dm³/s)
15	1.31	1.33	1.33
105	1.24	1.26	1.26
195	0.82	0.80	0.80
285	1.04	1.06	1.06

3.2.3 Turbulence model

Analysis of Tables 2 to 4 indicates that the most popular turbulence closure models used in NV simulation are the standard k–ε and the RNG k–ε models. For conciseness, this study used only the standard k–ε turbulence model. A set of exploratory runs (not included in this paper) showed that the results did not change significantly when using the RNG k–ε model.

3.2.4 Numerical scheme

The hybrid-differencing scheme (HDS) was used for all variables. This numerical scheme employs both the first-order upwind-differencing scheme (UDS), in high-convection regions, and the second-order central-differencing scheme (CDS), in low-convection regions.

3.2.5 Boundary conditions

The simulated wind directions are not always perpendicular to the domain's boundaries. Thus, two wind inlets are used to replicate the logarithmic wind profile used within the WT tests, in combination with two zero static pressure outlets on the opposite sides and top of the domain (van Hooff and Blocken 2013).

The lower boundary is modeled as fully-rough, to match the wind profile's surface roughness of 4.36 mm. All other solid objects that used for the building models are defined as smooth.

3.2.6 Model convergence

The flow field and equation residuals were monitored for each simulation, and for each time step, in the case of transient runs. Each simulation, or time step, was considered converged and was therefore concluded when a stationary flow field was obtained, with the residuals for all variables lower than 10^{-4} (Franke et al. 2007).

3.2.7 CFD outputs

Wind-driven pressures were obtained for 24 incoming wind directions in the same measurement positions used in the WT model.

Regarding the effective flow rates, comparison was performed for a scenario with all four windows opened (W1–W4 in Fig. 2). The CFD simulations used uniformly distributed non-buoyant heat as the tracing pollutant. After the source is turned off, the pollutant decay was evaluated in two points, located in the same positions as the two probes used in the WT measurements (P1 and P2). Transient simulations were required, due to the time-dependent nature of this method, as shown in Eq. (6). The equivalent pollutant decay equation when using non-buoyant heat is

shown in Eq. (8), which can be simplified, leading to Eq. (9):

$$\rho \times c_p \times [T(t) - T_{base}] = \rho \times c_p \times [T_0 - T_{base}] \times \exp\left(-\frac{\dot{V}}{V} \times t\right) \quad (8)$$

$$\Delta T(t) = \Delta T_0 \times \exp\left(-\frac{\dot{V}}{V} \times t\right) \quad (9)$$

The product of the slope of this function and the room's volume results in the effective airflow rate for that given location. Applying logarithms to Eq. (9) leads to a linear regression (Eq. (10)), which can be applied to the evolution of temperature difference through time:

$$\ln[\Delta T](t) = -\frac{\dot{V}}{V} \times t + \ln(\Delta T_0) \quad (10)$$

3.3 AFN simulations

The AFN approach was used to calculate wind-driven bulk airflow rates that were compared with CFD predictions. Using Eq. (3), the incoming airflow into the room was calculated for 24 incoming wind directions, using pressure coefficients from WT and CFD. As discussed above, bulk flow rates were not measured in the WT.

3.4 Relative average window opening area

The goal of this analysis is to calculate the average window opening area predicted by the three airflow modeling methods tested. The analysis compares the relative opening areas predicted for a given target wind driven flow rate. For this reason, the results obtained do not depend on the target flow rate. The calculations were performed for a whole year considering a 9-to-5 office occupation schedule and using two different wind scenarios:

- isotropic constant wind speed.
- TMY3 hourly wind data for San Francisco, based on the NREL dataset, recorded from 1973 to 2005 (Wilcox and Marion 2008).

3.5 Effects of window geometry

Due to the downscaling difficulties discussed above, the WT model used in this study has an unrealistically thick wall and modeled all windows as fully open holes. To make the analysis of the effects of window geometry more realistic, the CFD model used to assess the effect of window geometry on internal flow has a thinner wall (the scaled equivalent to a 0.17 m thickness). In cross-ventilated buildings with square apertures the air flows into the room as an approximately axis-symmetric jet (Carrilho da Graça et al. 2015). In contrast, most window geometries affect the flow field by deflecting incoming air towards a given location in the room (Heiselberg et al. 2001, 2002). To assess the impact of different window geometries on the effective flow, CFD simulations were performed for eight wind directions (0°–315°, in 45° intervals) using the same two sensor locations shown in Fig. 2. This analysis considered five different geometries:

- IB: window opens **inwards**, **bottom** opening axis
- IT: window opens **inwards**, **top** opening axis
- OB: window opens **outwards**, **bottom** opening axis
- OT: window opens **outwards**, **top** opening axis
- FO: fully open windows (**reference case**)

As can be seen in Fig. 5, a 25.1-degree tilted opening, which alters the direction of the airflow within the building, was added to each window of the first four geometries. Furthermore, this change in window geometry results in a 76% reduction in the effective opening area.

4 Validation results

This section presents the results of the validation, divided in four subsections focusing on: pressure coefficients, effective airflow rates, bulk airflow rates and discussion of results. In all subsections, the error indicators introduced in Section 2 are used to quantify the differences between the methods.

4.1 Pressure coefficients

Figure 6 shows a comparison between CFD and WT pressure coefficients for the 24 wind directions used in this study.

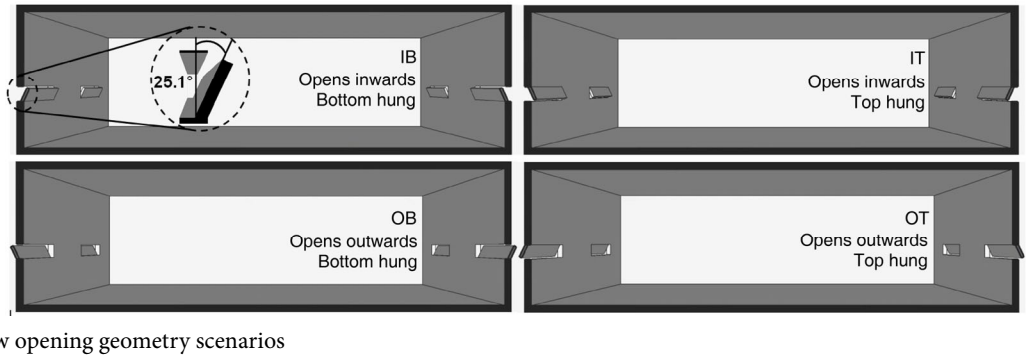

Fig. 5 Window opening geometry scenarios

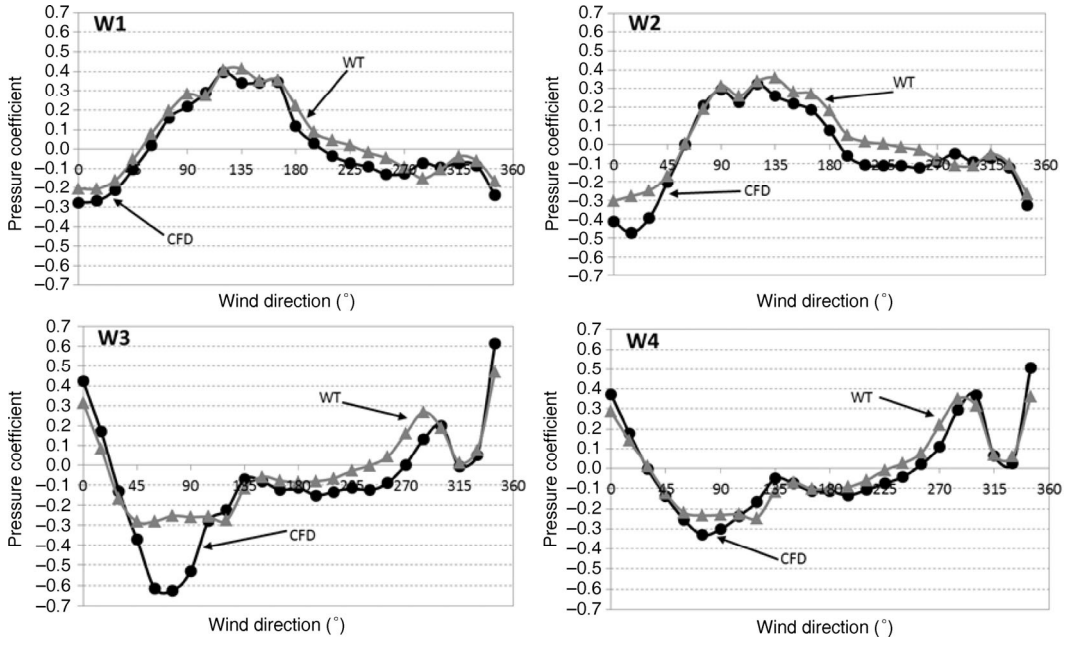

Fig. 6 Pressure coefficients for windows W1 to W4

The coefficient of correlation and the average error obtained in this comparison are shown in Table 7. Analysis of the results shows better agreement in the predictions for W1 and W4 (compared to W2 and W3). As can be seen in Fig. 2, W2 and W3 are closer to the edge of the building, a region where local recirculations and instability make CFD modeling more difficult. Still, the agreement obtained is better than a similar case analyzed by Zhang and Gu (2008) (a multi-incoming wind angle assessment of a building with surrounding buildings, R^2 of 0.420 and an average error of 47%). Overall, the error indicators are close to previous studies based on isolated buildings (R^2 between 0.847 and 0.995 and average error between 7% and 33%).

4.2 Effective airflow rates

Figure 7 presents a comparison between CFD and WT predictions of effective flow rates for 24 wind directions. The coefficient of correlation and the average error for this comparison are shown in Table 8. Analysis of the results reveals two levels of agreement, depending on the incoming wind direction:

- Wind directions between 195° and 30° lead to lower errors.
- Wind directions between 45° and 180° lead to larger errors.

For incoming wind between 195° to 30°, there is a good agreement: R^2 of 0.749, a result in the upper range of previously performed studies (see Table 3, R^2 between –0.296 and 0.963). The second group (45° to 180°) has a negative coefficient of determination, a result that also occurred in the study of Nikolopoulos et al. (2012). The average error for this group of wind directions is 37%, slightly above the review average (31%). The larger error might be the result of local flow instability near the openings (the wake of the larger surrounding buildings and the main building). Further, for these directions, the effective flow rate is overestimated, a problem that also occurred in a recent full scale CFD validation for a large building with lateral incoming wind in site with interfering surrounding buildings (Zhou et al. 2014). For all wind directions, the coefficient of determination is 0.628 and the average error is 32% (similar to the review average of 31%).

Table 7 R^2 and average error between wind tunnel and CFD pressure coefficients

Opening	R^2	Average error (%)
W1	0.920	30
W2	0.854	37
W3	0.776	48
W4	0.922	30
All windows	**0.836**	**37**
	Review average error	**35**

4.3 Bulk airflow rates

Bulk airflow rates were calculated with AFN and CFD models. AFN calculations used two alternative sources of pressure coefficients: WT and CFD. The bulk flow rates obtained with the AFN model, shown in Fig. 8, display a systematic under prediction. This effect was previously studied by

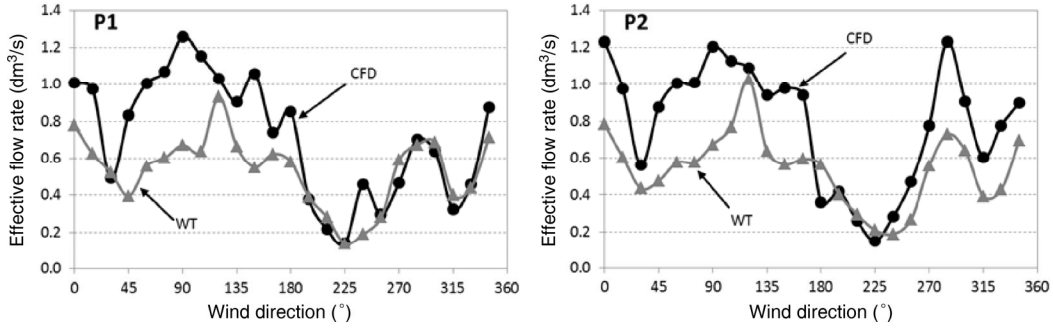

Fig. 7 Effective flow rates for measuring Points 1 and 2

Table 8 R^2 and average error between wind tunnel and CFD effective flow rates

Wind directions	Point	R^2	Average error (%)
195° to 30°	P1	0.736	19
	P2	0.886	33
	Average P1/P2	**0.749**	**27**
45° to 180°	P1	–0.957	37
	P2	–0.157	36
	Average P1/P2	**–0.436**	**37**
All directions	P1	0.564	30
	P2	0.703	35
	Average P1/P2	**0.628**	**32**
	Review average error		**31**

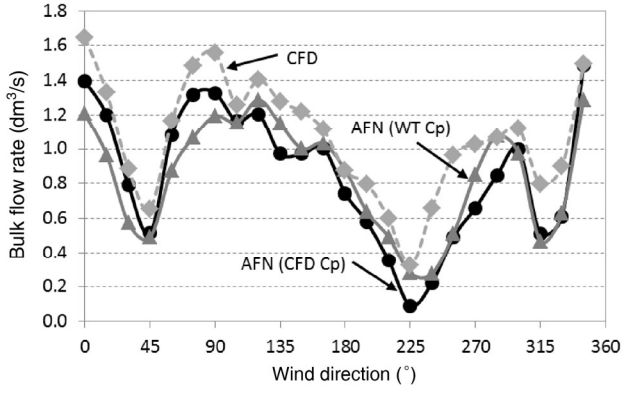

Fig. 8 Bulk flow rates

Karava et al. (2011), Kato et al. (1992) and later quantified by Carrilho da Graça (2003). According to these studies, AFN models cannot consider momentum conservation between inflow and outflow. This conservation effect leads to an increased bulk flow rate that cannot be predicted using the aperture-equation-based approach: for these cases CFD is the best option.

In spite of this systematic difference, bulk flow rate predictions display the lowest average errors obtained in this study (shown in Table 9). Clearly, the square root dependence

Table 9 R^2 and average error between AFN and CFD bulk flow rates

Method	R^2	Average error (%)
AFN (CFD C_p)/AFN (WT C_p)	0.851	14
AFN (CFD C_p)/CFD	0.729	20
AFN (WT C_p)/CFD	0.734	21
Review average error		**23**

(Eq. (3)) of the bulk airflow rate on the wind generated pressure difference reduces the impact of existing errors of the pressure coefficients. Further, these calculations use, simultaneously, the pressure coefficients for all four windows, thereby averaging the impact from individual errors. Both the average error (20%) and the R^2 obtained are comparable to the review average (23%, and 0.679–0.944).

4.4 Discussion

Table 10 shows a comparison between the results obtained in this study and existing studies. In all cases the errors obtained are similar to the average of existing studies. For prediction of pressure coefficients RANS CFD displayed good agreement with WT measurements, with a coefficient of determination of 0.84 and average normalized error of 37%. The highest discrepancies occur in surfaces that are exposed to flow recirculations generated in the wake of large adjacent buildings. The results obtained for effective flow rate display low accuracy for incoming wind directions between 45° and 180°, with a 37% average error and a negative coefficient of determination. This wind quadrant has adjacent buildings that are closer to the NV office. Further, the use of only two sensor locations in the room may contribute to these differences, as any imprecision in the prediction of the inflow jet angle will have a relevant impact in the results. Bulk airflow rates produced the lowest average errors: 21% when comparing CFD to AFN with WT C_p. This decrease is a direct consequence of the proportionality between airflow rate and the square root of the pressure difference.

Table 10 Summary of error indicators obtained for this study and existing studies

Variable	Tool	Average error	
		This study (%)	Review (%)
Pressure coefficients (C_p)	CFD	37	35
Bulk flow rate	CFD&AFN	21	23
Effective flow rate	CFD	32	31

5 Impacts in window design

This section presents an analysis of the impacts of the models in NV design. It begins with an analysis of predicted average window opening area and concludes with an evaluation of effects of detailed window geometry.

5.1 Average window opening area

The analysis of average window opening area used two different wind profiles: isotropic constant wind, and hourly San Francisco wind data (TMY file). Figure 9 shows the occurrence distribution of wind by speed and direction for San Francisco, revealing a predominance of winds in the 255° to 315° quadrant. This asymmetric distribution increases the cumulative impact of differences in predicted flow rate for these wind directions. Therefore, the lower flow rate differences that were found for that range of wind directions are expected to decrease the discrepancy between the calculated opening areas. The relative average window opening predicted is shown in Table 11. WT is the reference for effective flow rate predictions, whereas for bulk flow rate the reference is AFN with WT pressure coefficients.

For both scenarios, the WT based flow rates results in the highest average window opening area, a direct consequence of the lower flow rates predicted for most wind directions (Fig. 7). The larger discrepancy is found in the AFN (WT C_p)/ CFD comparison: in this case the larger flows predicted by

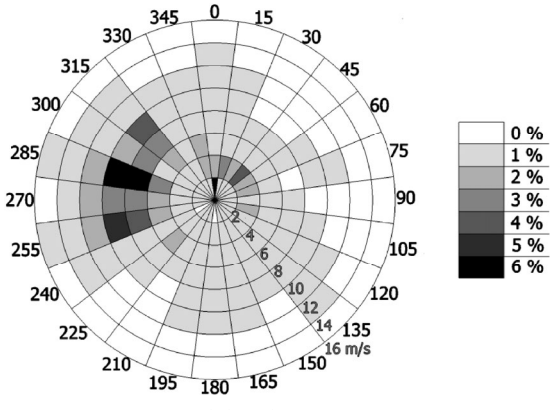

Fig. 9 San Francisco wind distribution

Table 11 Relative average window opening area

Wind data	Effective flow rate (%)		Bulk flow rate (%)		
	WT	CFD	AFN (WT C_p)	AFN (CFD C_p)	CFD
Isotropic (constant wind)	100	80	100	82	61
San Francisco	100	74	100	91	67

CFD result in a 30%–40% reduction in predicted window area. The impact of the local distribution of wind by speed and direction on the predictions is not significant (variations of less than 10%).

5.2 Window geometry effect

Figure 10 shows the predicted variations of average effective flow rate obtained in points P1 and P2 for the four different window geometries shown in Fig. 5. Table 12 presents the effective flow rate results normalized using the reference fully open (FO) window effective flow result. In all cases studied, inclusion of detailed window geometry leads, on average, to an increase in the effective flow rate due to improved mixing of the room air (in some wind angles up to 30%). Clearly, a complete NV design analysis should include the effects of flow deflection by partially open windows.

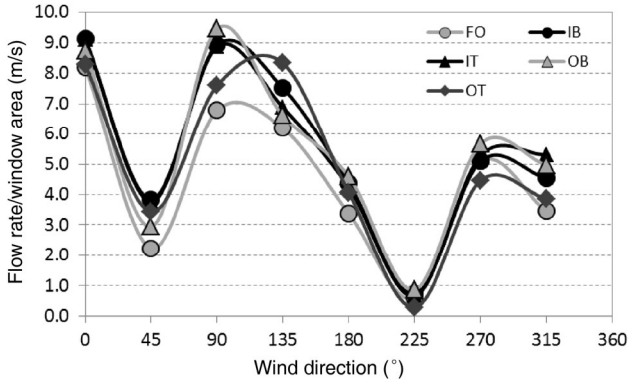

Fig. 10 Average effective (decay method) flow rates per window opening area for different window strategies

Table 12 Average variation between fully open and each other window opening scenario

Case	Average difference from FO (%)
IB	+19
IT	+19
OB	+18
OT	+16
Average	**+18**

6 Conclusions

This paper presented a validation of AFN and RANS CFD simulations for a naturally ventilated office building. The validation was based on WT measurements of wind generated pressure coefficients and effective airflow rates. The results are in line with existing comparisons, confirming that RANS CFD produces precise results for head-on incoming wind in buildings with most ventilation apertures concentrated on the windward and leeward sides. For wind angles that are parallel to the aperture planes, the precision is lower, confirming the know difficulties of RANS CFD simulations in shear-driven flows with recirculations.

For simple isolated buildings, RANS CFD can predict pressure coefficients with less than 20% average error. For complex geometries average error is less than 40%. Bulk flow rates depend on the square root of the pressure coefficients. For this reason, errors in this quantity are lower, typically less than 25%. Further, due to its capability to account for the momentum conservation effects that occur in cross-ventilation, CFD may be the most precise method for bulk flow rate predictions.

Effective flow rates are the most relevant quantity to evaluate the efficiency of NV designs. Unfortunately, the error in RANS CFD predictions for this quantity can be as high as 40%. Yet, CFD can model detailed window effects that, in some cases, can change the effective flow rate in 30% (20% on average). Most NV design cases have partially open windows that deflect the flow. For these cases the precision of an effective flow rate RANS CFD prediction can be comparable to a WT study since the inherent modeling error being can be compensated by the capability to model detailed window effects.

The results obtained indicate that RANS CFD has reached a development stage that makes it a candidate for use as an accessible and flexible virtual wind tunnel, either producing pressure coefficients for AFN models or predicting the whole flow field in particular wind directions and window configurations. For isolated buildings RANS CFD may already be preferable to WT due to its increased capability to model window geometry and analyze internal flow features.

Acknowledgements

The authors would like to thank Dr. David Banks (CPP Wind) for providing the wind tunnel data used in this study. The authors would also like to thank Dr. Nicolas Daish and Dr. Spencer Dutton for the fruitful discussions about the simulation tools used in this study. The authors would also like to thank the California Energy Commission (*Natural ventilation for energy savings in California commercial buildings*, contract 500-10-025) and Fundação para a Ciência e Tecnologia (MIT-Portugal Program, SFRH/BD/52084/2013) for providing financial support.

References

Anderson Jr. JD (1995). Computational Fluid Dynamics: The Basics with Applications. New York: McGraw-Hill.

Asfour OS, Gadi MB (2007). A comparison between CFD and network models for predicting wind-driven ventilation in buildings. *Building and Environment*, 42: 4079–4085.

Awbi H (2003). Ventilation of Buildings. New York: Spon Press.

Axley J (2007). Multizone airflow modeling in buildings: History and theory. *HVAC&R Research*, 13: 907–928.

Belleri A, Lollini L, Dutton SM (2014). Natural ventilation design: An analysis of predicted and measured performance. *Building and Environment*, 81: 123–138.

Bitsuamlak B (2006). Application of computational wind engineering: A practical perspective. In: Proceedings of 3rd National Conference in Wind Engineering, Kolkata, India.

Blocken B (2014). 50 years of computational wind engineering: Past, present and future. *Journal of Wind Engineering and Industrial Aerodynamics*, 129: 69–102.

Calautit JK, Hughes BR (2014). Wind tunnel and CFD study of the natural ventilation performance of a commercial multi-directional wind tower. *Building and Environment*, 80: 71–83.

California Building Standards Commission (2013). California Building Standards Code, California Code of Regulations, Title 24.

Carrilho da Graça G (2003). Simplified models for heat transfer in rooms. PhD Dissertation, University of California, San Diego, USA.

Carrilho da Graça G, Linden PF, Haves P (2004). Design and testing of a control strategy for a large, naturally ventilated office building. *Building Services Engineering Research and Technology*, 25: 223–239.

Carrilho da Graça G, Martins NR, Horta CS (2012). Thermal and airflow simulation of a naturally ventilated shopping mall. *Energy and Buildings*, 50: 177–188.

Carrilho da Graça G, Daish NC, Linden PF (2015). A two-zone model for natural cross-ventilation. *Building and Environment*, 89: 72–85.

Cermak JE (1971). Laboratory simulation of the atmospheric boundary layer. *AIAA Journal*, 9: 1746–1754.

Cermak JE (1975). Applications of fluid mechanics to wind engineering. *Journal of Fluids Engineering*, 97: 9–38.

Cermak JE (1976). Aerodynamics of Buildings. *Annual Review of Fluid Mechanics*, 8: 75–106.

CHAM Ltd. (2012). PHOENICS 2011 (64bit Intel 17/06/2012). London.

Chen Q (1995). Comparison of different k–ε models for indoor air flow computations. *Numerical Heat Transfer*, *Part B*: *Fundamentals*, 28: 353–369.

Chen Q (2009). Ventilation performance prediction for buildings: A method overview and recent applications. *Building and Environment*, 44: 848–858.

Cheung JOP, Liu C-H (2011). CFD simulations of natural ventilation behaviour in high-rise buildings in regular and staggered arrangements at various spacings. *Energy and Buildings*, 43: 1149–1158.

Cochran L, Derickson R (2011). A physical modeler's view of computational wind engineering. *Journal of Wind Engineering and Industrial Aerodynamics*, 99: 139–153.

CPP Wind (2015). CPP Wind Engineering & Air Quality Experts, CPP Wind Engineering & Air Quality Consulting for Building Design. Available at http://www.cppwind.com.

Crawley DB, Lawrie LK, Winkelmann FC, Buhl WF, Joe Huang Y, Pedersen CO, Strand RK, Liesen RJ, Fisher DE, Witte MJ, Glazer J (2001). EnergyPlus: Creating a new-generation building energy simulation program. *Energy and Buildings*, 33: 319–331.

Dutton SM, Banks D, Brunswick SL, Fisk WJ (2013). Health and economic implications of natural ventilation in California offices. *Building and Environment*, 67: 34–45.

Evola E, Popov V (2006). Computational analysis of wind driven natural ventilation in buildings. *Energy and Buildings*, 38: 491–501.

Franke J, Hellsten A, Schlünzen H, Carissimo B (2007). Best practice guideline for the CFD simulation of flows in the urban environment. Brussels: COST Office.

Glória Gomes M, Moret Rodrigues A, Mendes P (2005). Experimental and numerical study of wind pressures on irregular-plan shapes. *Journal of Wind Engineering and Industrial Aerodynamics*, 93: 741–756.

Heiselberg P, Svidt K, Nielsen PV (2001). Characteristics of airflow from open windows. *Building and Environment*, 36: 859–869.

Heiselberg P, Bjørn E, Nielsen PV (2002). Impact of open windows on room air flow and thermal comfort. *International Journal of Ventilation*, 1: 91–100.

Lo JL, Banks D, Novoselac A (2013). Combined wind tunnel and CFD analysis for indoor airflow prediction of wind-driven cross ventilation. *Building and Environment*, 60: 12–23.

Jiang Y, Chen Q (2002). Effect of fluctuating wind direction on cross natural ventilation in buildings from large eddy simulation. *Building and Environment*, 37: 379–386.

Jiang Y, Alexander D, Jenkins H, Arthur R, Chen Q (2003). Natural ventilation in buildings: Measurement in a wind tunnel and numerical simulation with large-eddy simulation. *Journal of Wind Engineering and Industrial Aerodynamics*, 91: 331–353.

Karava P, Stathopoulos T, Athienitis AK (2011). Airflow assessment in cross-ventilated buildings with operable facade elements. *Building and Environment*, 46: 266–279.

Kato S, Murakami S, Mochida A, Akabayashi S-I, Tominaga Y (1992). Velocity-pressure field of cross ventilation with open windows analyzed by wind tunnel and numerical simulation. *Journal of Wind Engineering and Industrial Aerodynamics*, 44: 2575–2586.

Kobayashi T, Sandberg M, Kotani H, Claesson L (2010). Experimental investigation and CFD analysis of cross-ventilated flow through single room detached house model. *Building and Environment*, 45: 2723–2734.

Labat M, Woloszyn M, Garnier G, Roux JJ (2013). Assessment of the air change rate of airtight buildings under natural conditions using the tracer gas technique. Comparison with numerical modelling. *Building and Environment*, 60: 37–44.

Linden PF (1999). The fluid mechanics of natural ventilation. *Annual Review of Fluid Mechanics*, 31: 201–238.

Liu X, Niu J, Kwok KCS (2013). Evaluation of RANS turbulence models for simulating wind-induced mean pressures and dispersions around a complex-shaped high-rise building. *Building Simulation*, 6: 151–164.

Montazeri H, Blocken B (2013). CFD simulation of wind-induced pressure coefficients on buildings with and without balconies: Validation and sensitivity analysis. *Building and Environment*, 60: 137–149.

Nikas K-S, Nikolopoulos N, Nikolopoulos A (2010). Numerical study of a naturally cross-ventilated building. *Energy and Buildings*, 42: 422–434.

Nikolopoulos N, Nikolopoulos A, Larsen TS, Nikas K-SP (2012). Experimental and numerical investigation of the tracer gas methodology in the case of a naturally cross-ventilated building. *Building and Environment*, 56: 379–388.

Richards PJ, Norris SE (2011). Appropriate boundary conditions for computational wind engineering models revisited. *Journal of Wind Engineering and Industrial Aerodynamics*, 99: 257–266.

Seifert J, Li Y, Axley J, Rösler M (2006). Calculation of wind-driven cross ventilation in buildings with large openings. *Journal of Wind Engineering and Industrial Aerodynamics*, 94: 925–947.

Seppänen O, Fisk WJ (2002). Association of ventilation system type with SBS symptoms in office workers. *Indoor Air*, 12: 98–112.

Shen X, Zhang G, Bjerg B (2012). Comparison of different methods for estimating ventilation rates through wind driven ventilated buildings. *Energy and Buildings*, 54: 297–306.

Teppner R, Langensteiner B, Meile W, Brenn G, Kerschbaumer S (2014). Air change rates driven by the flow around and through a building storey with fully open or tilted windows: An experimental and numerical study. *Energy and Buildings*, 76: 640–653.

Tominaga Y, Mochida A, Murakami S, Sawaki S (2008a). Comparison of various revised k–ε models and LES applied to flow around a high-rise building model with 1:1:2 shape placed within the surface boundary layer. *Journal of Wind Engineering and Industrial Aerodynamics*, 96: 389–411.

Tominaga Y, Mochida A, Yoshie R, Kataoka H, Nozu T, Yoshikawa M, Shirasawa T (2008b). AIJ guidelines for practical applications of CFD to pedestrian wind environment around buildings. *Journal of Wind Engineering and Industrial Aerodynamics*, 96: 1749–1761.

United States Environmental Protection Agency (1981). Guideline for Fluid Modeling of Atmospheric Diffusion, United States Environmental Protection Agency, Report EPA-600/8-81-009.

van Hooff T, Blocken B, Aanen L, Bronsema B (2011). A venturi-shaped roof for wind-induced natural ventilation of buildings: Wind tunnel and CFD evaluation of different design configurations. *Building and Environment*, 46: 1797–1807.

van Hooff T, Blocken B (2013). CFD evaluation of natural ventilation of indoor environments by the concentration decay method: CO_2 gas dispersion from a semi-enclosed stadium. *Building and Environment*, 61: 1–17.

Wilcox S, Marion W (2008). User's Manual for TMY3 Datasets, NREL/TP-581-43156. Colorado: National Renewable Energy Laboratory.

Zhang A, Gu M (2008). Wind tunnel tests and numerical simulations of wind pressures on buildings in staggered arrangement. *Journal of Wind Engineering and Industrial Aerodynamics*, 96: 2067–2079.

Zhou C, Wang Z, Chen Q, Jiang Y, Pei J (2014). Design optimization and field demonstration of natural ventilation for high-rise residential buildings. *Energy and Buildings*, 82: 457–465.